Comp. Meth. Civil Eng, Vol. 2, 2 (2011) 219-230

CMCE
Computational Methods in Civil Engineering

Axial buckling analysis of an isotropic cylindrical shell using the meshless local Petrov-Galerkin method

A. Arjangpay, M. Darvizeh, R. Ansari*, Gh. Zarepour

Department of Mechanical Engineering, University of Guilan, P.O. Box 3756, Rasht, Iran

Received 13 September 2011; accepted in revised form 11 December 2011

Abstract

In this paper the meshless local Petrov-Galerkin (MLPG) method is implemented to study the buckling of isotropic cylindrical shells under axial load. Displacement field equations, based on Donnell and first order shear deformation theory, are taken into consideration. The set of governing equations of motion are numerically solved by the MLPG method in which according to a semi-inverse method, a new variational trial-functional is constructed to derive the stiffness matrices and critical buckling loads are obtained in various boundary conditions.

The moving least squares interpolation is employed to construct both trial and test functions. The present method is a truly meshless method based on a number of randomly located nodes upon which no global background integration mesh is needed and no element matrix assembly is required. In the present MLPG formulation, a local variational form is constructed over a local sub-domain instead of using the conventional weighted-residual procedure. The influences of some commonly used boundary conditions and effects of shell geometrical parameters are studied. The results show the convergence characteristics and accuracy of the mentioned method.

Keywords: Axial buckling; Isotropic cylindrical shells; MLPG method.

1. Introduction

In recent years there is a growing interest in the meshless methods, which do not require a finite element mesh for the definition of the approximation and decrease the difficulties caused by meshing and remeshing. Because of the high order of continuity of meshless approximation functions, meshless methods can express the face and displacement of a shell very well.

Several meshless methods have been reported in the literature, such as the smooth particle hydrodynamics (SPH) [1] to which the initial idea of meshless methods dates back, the diffuse element [2], the element-free Galerkin (EFG) [3], the reproducing kernel particle method (RKPM) [4], hp-clouds [5], the partition of unity method (PUM) [6], the natural

*Corresponding author.
Fax +98 131 6690271.
E-mail address: r_ansari@Guilan.ac.ir (R. Ansari).

element method (NEM) [7] and the meshless local Petrov–Galerkin (MLPG) [8,9]. The major difference in these meshless methods comes from the interpolation techniques used. These methods, except for the MLPG which is local in character, need shadow elements to evaluate the domain integrals over the entire domain of the problem. As a matter of fact, the background cell integration does not lead to a truly meshless method. The major contribution of the MLPG method is its establishment based on the local weak form for which no background mesh is required to numerically evaluate the integrands in the MLPG formulation. This means that the weak form is satisfied at each node in the problem domain in a local integral sense. Accordingly, the MLPG method is regarded as a truly meshless method not only in terms of the non-element interpolation, but also in terms of the non-mesh integration. It can also include the other meshless methods based on global formulation, as special cases. In the MLPG formulation, test functions may be chosen from a different space than the space of trial solutions. Since the MLPG concept is a general framework to formulate various meshless methods with a greater degree of flexibility, variants of the MLPG formulation labeled as MLPG1 – MLPG6 for different trial-function interpolant schemes, or different choices of test functions have been appeared in the literature [10,11]. The present method is also more flexible and easier in dealing with nonlinear problems than the conventional FEM, EFG and BEM. Furthermore, for the same accuracy, the computational cost in MLPG can be also lower than that in the FEM. Thus, the MLPG method, due to its speed, accuracy and robustness, has shown a great promise in engineering applications and may be expected to replace the FEM in the near future [10]. Cylindrical shells are commonly used in practical engineering such as underground mining, subsurface building and petrol conveying. The main purpose of the present study is to predict axial buckling characteristics of isotropic cylindrical shells with arbitrary boundary conditions.

2. Field equations for isotropic shells

2.1. Kinematics relations

Based on the first order shear deformation (FOSD) theory, the three-dimensional displacement components u, v and w in the x, θ and z directions respectively, as shown in Figure 1, are assumed to be

$$\begin{aligned} u_x(x,\theta,z) &= u(x,\theta) + z\psi_x(x,\theta) \\ u_\theta(x,\theta,z) &= v(x,\theta) + z\psi_\theta(x,\theta) \\ u_z(x,\theta,z) &= w(x,\theta) \end{aligned} \tag{1}$$

where u, v, w are the reference surface displacements and ψ_x, ψ_θ are the rotations of transverse normal about the x-and θ-axes, respectively. The middle surface strains ε_x, ε_θ and $\varepsilon_{x\theta}$ the shear strains γ_{xz} and $\gamma_{\theta z}$ and the middle surface curvature k_x, k_θ and $k_{x\theta}$ are given by

$$\begin{bmatrix} \varepsilon_x \\ \varepsilon_\theta \\ \varepsilon_{x\theta} \\ k_x \\ k_\theta \\ k_{x\theta} \\ \gamma_{xz} \\ \gamma_{\theta z} \end{bmatrix} = \begin{bmatrix} \frac{\partial}{\partial x} & 0 & 0 & 0 & 0 \\ 0 & \frac{1}{R}\frac{\partial}{\partial \theta} & \frac{1}{R} & 0 & 0 \\ \frac{1}{R}\frac{\partial}{\partial \theta} & \frac{\partial}{\partial x} & 0 & 0 & 0 \\ 0 & 0 & 0 & \frac{\partial}{\partial x} & 0 \\ 0 & 0 & 0 & 0 & \frac{1}{R}\frac{\partial}{\partial \theta} \\ 0 & 0 & 0 & \frac{1}{R}\frac{\partial}{\partial \theta} & \frac{\partial}{\partial x} \\ 0 & 0 & \frac{\partial}{\partial x} & 1 & 0 \\ 0 & -\frac{1}{R} & \frac{1}{R}\frac{\partial}{\partial \theta} & 0 & 1 \end{bmatrix} \begin{bmatrix} u \\ v \\ w \\ \psi_x \\ \psi_\theta \end{bmatrix} \tag{2}$$

2.2. Stress resultant-strain relations

The force and moment intensities for cylindrical shear deformation, can be found in following form [12]

$$\begin{bmatrix} N_x \\ N_\theta \\ N_{x\theta} \\ M_x \\ M_\theta \\ M_{x\theta} \\ Q_x \\ Q_\theta \end{bmatrix} = \begin{bmatrix} A & \nu A & 0 & 0 & 0 & 0 & 0 & 0 \\ \nu A & A & 0 & 0 & 0 & 0 & 0 & 0 \\ 0 & 0 & \frac{(1-\nu)A}{2} & 0 & 0 & 0 & 0 & 0 \\ 0 & 0 & 0 & D & \nu D & 0 & 0 & 0 \\ 0 & 0 & 0 & \nu D & D & 0 & 0 & 0 \\ 0 & 0 & 0 & 0 & 0 & \frac{(1-\nu)D}{2} & 0 & 0 \\ 0 & 0 & 0 & 0 & 0 & 0 & Gh & 0 \\ 0 & 0 & 0 & 0 & 0 & 0 & 0 & Gh \end{bmatrix} \begin{bmatrix} \varepsilon_x \\ \varepsilon_\theta \\ \varepsilon_{x\theta} \\ k_x \\ k_\theta \\ k_{x\theta} \\ \gamma_{xz} \\ \gamma_{\theta z} \end{bmatrix} \tag{3}$$

in which

$$A = \frac{Eh}{1-\nu^2}, D = \frac{Eh^3}{12(1-\nu^2)}, G = \frac{E}{2(1+\nu)} \tag{4}$$

where E and υ are Young's modulus and Poisson's ratio respectively.

2.3. Cylindrical shell equations

Consider a cylindrical elastic shell of radius R, length L, thickness h, as shown in Figure 1. If x and θ represent the longitudinal and circumferential coordinates respectively the governing equations on the basis of the Donnell shell theory are given as [12]

$$\begin{aligned} &\frac{\partial N_{xx}}{\partial x} + \frac{1}{R}\frac{\partial N_{\theta x}}{\partial \theta} = 0 \\ &\frac{\partial N_{x\theta}}{\partial x} + \frac{1}{R}\frac{\partial N_{\theta\theta}}{\partial \theta} + \frac{Q_{\theta\theta}}{R} = 0 \\ &\frac{\partial Q_{xx}}{\partial x} + \frac{1}{R}\frac{\partial Q_{\theta\theta}}{\partial \theta} - \frac{N_{\theta\theta}}{R} - \widetilde{N}_x \frac{\partial^2 w}{\partial x^2} = 0 \\ &\frac{\partial M_{xx}}{\partial x} + \frac{1}{R}\frac{\partial M_{x\theta}}{\partial \theta} - Q_{xx} = 0 \\ &\frac{\partial M_{x\theta}}{\partial x} + \frac{1}{R}\frac{\partial M_{\theta\theta}}{\partial \theta} - Q_{\theta\theta} = 0 \end{aligned} \tag{5}$$

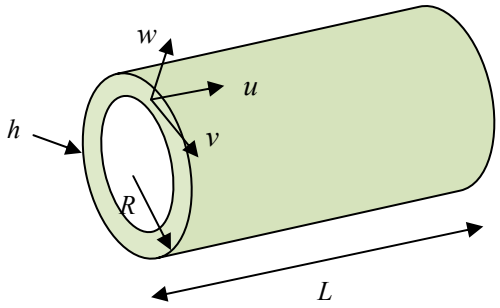

Figure 1. Coordinate system and shell geometry.

2.4. Variational form of the field equations

Constructing the underlying quadratic functional of the shell theory is not a straightforward procedure. Thus, a semi-inverse method [13-15] is used to construct a variational trial-functional of the form $\Pi(u,v,w,\psi_x,\psi_\theta)$ as follows

$$\Pi = \Pi_K(u,v,w,\psi_x,\psi_\theta) + \Pi_{K_g}(u,v,w,\psi_x,\psi_\theta) \tag{6}$$

$$\Pi_K(u,v,w,\psi_x,\psi_\theta) = \frac{1}{2}\int_\Omega \Bigg(\left[\frac{Eh}{1-\nu^2}u_{,x} + \frac{1}{R}\frac{\nu Eh}{1-\nu^2}(v_{,\theta}+w) \right] u_{,x} + \frac{Eh}{2(1+\nu)}\left(\frac{u_{,\theta}}{R}+v_{,x}\right)^2 +$$

$$\left[\frac{\nu Eh}{1-\nu^2}u_{,x} + \frac{1}{R}\frac{Eh}{1-\nu^2}(v_{,\theta}+w) \right]\frac{1}{R}(v_{,\theta}+w) + D\left(\psi_{x,x}+\frac{\nu}{R}\psi_{\theta,\theta}\right)\psi_{x,x} + \tag{7}$$

$$\frac{D}{R}\left(\frac{1}{R}\psi_{\theta,\theta}+\nu\psi_{x,x}\right)\psi_{\theta,\theta} + \frac{(1-\nu)D}{2}(\psi_{x,\theta}-\psi_{\theta,x})^2 + \frac{Eh}{2(1+\nu)}(w_{,x}+\psi_x)^2 + \frac{Eh}{2(1+\nu)}\left(-\frac{v}{R}+\frac{w_\theta}{R}+\psi_\theta\right)^2 \Bigg) d\Omega$$

$$\Pi_{K_g}(u,v,w,\psi_x,\psi_\theta) = \frac{1}{2}\int_\Omega \widetilde{N}_x (w_{,x})^2 \, d\Omega \tag{8}$$

in which $\widetilde{N}_x$ presents axial buckling load.

3. Solution procedure

3.1. The MLPG method and MLS interpolation

The MLPG method, based on a local formulation, can include all the other meshless methods based on a global formulation, as special cases, if the trial and test functions and the integration methods are selected appropriately. In the MLPG, the nodal trial and test functions can be different. Herein the moving least squares (MLS) approximation is chosen as both trial and test functions. Employing MLS, a function $v(x)$ in a domain Ω can be approximated by $v^h(x)$ in the sub-domain Ω_x and

$$v^h(x) = \sum_{i=1}^{m} q_i(x) b_i(x) = q^T(x) b(x) \tag{9}$$

where $q_i(x)$ are the monomial basis functions, $b_i(x)$ are the corresponding coefficients, h is a factor that measures the domain of influence of the nodes and m is the number of basis functions. The commonly used basis functions are the polynomial, such as:

$$q^T = \left[1, x, x^2, x^3\right],\ m = 4 \tag{10}$$

In this method, we use the quadratic basis. The unknown coefficients $b_i(x)$ are obtained by the minimization of a weighted discrete L_2 norm

$$\Gamma = \sum_{I=1}^{n} \omega(x - x_I)(q^T(x_I)b(x) - v_I)^2 \tag{11}$$

where $\omega(x - x_I)$ or $\omega(x_I)$ is the weight function that is associated with node I, $\omega(x_I) = 0$ outside Ω_x, n is the number of nodes in Ω_x that makes the weight function $\omega(x_I) \succ 0$ and v_I are the nodal parameters. The minimization of Γ in equation (11) with respect to $b(x)$ leads to a set of linear equations

$$B(x)b(x) = A(x)v \tag{12}$$

where

$$B(x) = \sum_{I=1}^{n} \omega(x - x_I)q(x_I)q^T(x_I) \tag{13}$$

and

$$A(x) = \left[\omega(x - x_1)q(x_1), ..., \omega(x - x_n)q(x_n)\right] \tag{14}$$

The coefficients b(x) are then derived from equation (12)

$$b(x) = B^{-1}(x)A(x)v \tag{15}$$

By substituting equation (15) into equation (9), the approximation $v^h(x)$ is expressed in a standard form as

$$v^h(x) = \sum_{I=1}^{n} N_I(x)v_I \tag{16}$$

where the shape function $N_I(x)$ is given by

$$N_I(x) = q^T(x)B^{-1}(x)A_I(x) \tag{17}$$

From equation (13), we obtain

$$A_I(x) = \omega(x - x_I)q_I(x) \tag{18}$$

and thus equation (17) can be rewritten as

$$N_I(x) = q^T(x)B^{-1}(x)q_I(x)\omega(x - x_I) \tag{19}$$

A cubic spline function

$$\omega(s) = \begin{cases} \frac{2}{3} - 4s^2 + 4s^3, & s \le \frac{1}{2} \\ \frac{4}{3} - 4s + 4s^2 - \frac{4}{3}s^3, & \frac{1}{2} < s \le 1 \\ 0, & s > 1 \end{cases}, s = \frac{|x - x_I|}{d_w} \tag{20}$$

can be used as the weight function.

In the conventional MLPG method, weighted residual is often used to create the system of discrete equations. In the present MLPG formulation a local variational form is constructed over a local sub-domain instead of using the conventional weighted-residual procedure. The local sub-domains covering the whole global domain are located entirely within the global domain and may overlap each other. The sub domain is taken to be a circle, a rectangle, or an ellipse in two dimensions centered at a node x_i. The main idea of MLPG is that the variational form is satisfied at each node in the problem domain in a local integral sense.

For applying the MLPG method on shell theory, a one dimensional problem is considered in which the domain is discretized by a set of regular distributed nodes, as in Figure 2. The mass and stiffness matrices are obtained from the corresponding variational forms constructed. The present MLPG formulation leads to symmetric matrices, as in FEM, without requiring an assembly process.

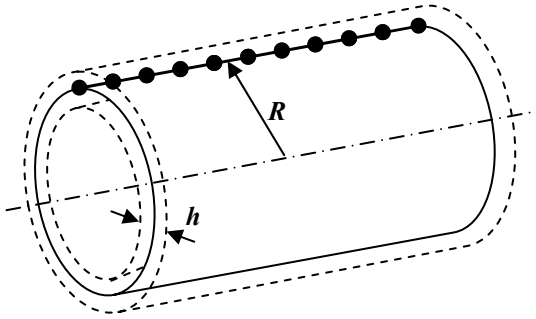

Figure 2. Schematics of nodes arrangement on the shell.

3.2. Discretization procedure

The field variables can be expressed in the circumferential direction by the Fourier series as

$$\begin{aligned} u(x,\theta) &= U(x)\cos(n\theta) \\ v(x,\theta) &= V(x)\sin(n\theta) \\ w(x,\theta) &= W(x)\cos(n\theta) \\ \psi_x(x,\theta) &= \Psi_x(x)\cos(n\theta) \\ \psi_\theta(x,\theta) &= \Psi_\theta(x)\sin(n\theta) \end{aligned} \tag{21}$$

where n is circumferential mode number and $U(x), V(x), W(x), \Psi_x(x)$ and $\Psi_\theta(x)$ are axial modal functions. By introducing the foregoing equations into the variational statements given by equations (6-8), discretizing the resulting equations by the MLPG method and then recasting them into a generalized eigenvalue problem, one would arrive at

$$\left([K]-\tilde{N}_x[K_g]\right)\{X\}=0 \tag{22}$$

where the nodal vector $\{X\}$ is defined as

$$X=\begin{bmatrix} u & v & w & \psi_x & \psi_\theta \end{bmatrix} \tag{23}$$

And the stiffness matrix K and geometrical stiffness matrix K_g in equation (22) are given by

$$K=\frac{1}{2}\pi R\int_{\Omega} B^T DB dx \tag{24}$$

$$K_g = \frac{1}{2}\pi R \int_{\Omega} G^T J G dx \tag{25}$$

in which

$$B = \begin{bmatrix} N_{I,x} & 0 & 0 & 0 & 0 \\ 0 & \frac{n}{R}N_I & \frac{1}{R}N_I & 0 & 0 \\ -\frac{n}{R}N_I & N_{I,x} & 0 & 0 & 0 \\ 0 & 0 & 0 & N_{I,x} & 0 \\ 0 & 0 & 0 & 0 & \frac{n}{R}N_I \\ 0 & 0 & 0 & -\frac{n}{R}N_I & N_{I,x} \\ 0 & 0 & N_{I,x} & N_I & 0 \\ 0 & -\frac{1}{R}N_I & -\frac{n}{R}N_I & 0 & N_I \end{bmatrix} \tag{26}$$

and

$$D = \begin{bmatrix} A & \nu A & 0 & 0 & 0 & 0 & 0 & 0 \\ \nu A & A & 0 & 0 & 0 & 0 & 0 & 0 \\ 0 & 0 & \frac{(1-\nu)A}{2} & 0 & 0 & 0 & 0 & 0 \\ 0 & 0 & 0 & D & \nu D & 0 & 0 & 0 \\ 0 & 0 & 0 & \nu D & D & 0 & 0 & 0 \\ 0 & 0 & 0 & 0 & 0 & \frac{(1-\nu)D}{2} & 0 & 0 \\ 0 & 0 & 0 & 0 & 0 & 0 & Gh & 0 \\ 0 & 0 & 0 & 0 & 0 & 0 & 0 & Gh \end{bmatrix} \tag{27}$$

$$G = \begin{bmatrix} 0 & 0 & N_{I,x} & 0 & 0 \\ 0 & 0 & -\frac{n}{R}N_I & 0 & 0 \end{bmatrix} \tag{28}$$

$$J = \begin{bmatrix} 1 & 0 \\ 0 & 0 \end{bmatrix} \tag{29}$$

where E and υ are Young's modulus and Poisson's ratio, respectively. Moreover, the interpolation function N_I can be constructed by the MLS approximation.

A numerical integration is needed to evaluate the integration in Eqs.(24)-(25). The gauss quadrature is used in the MLPG. For a node x_i a local integration domain is needed to employ Gauss quadrature. For each Gauss quadrature point x_Q, the point interpolation is performed to obtain the integrand. Therefore, as shown in the Figure 3, for node x_i there exist three local domains: local integration domain, test function domain, and interpolation domain for x_Q. It should be noted that the integration domain and test function domain are considered to be the same.

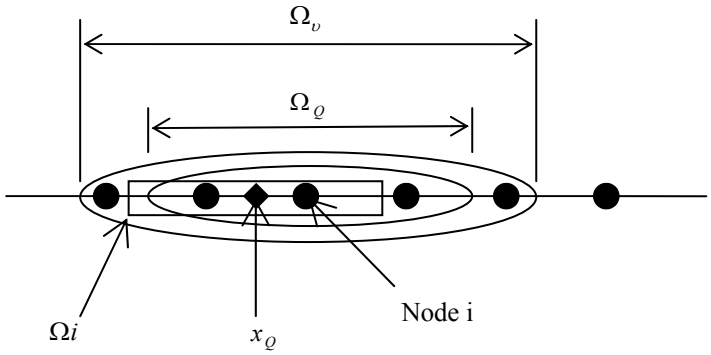

Figure 3. The support domain Ω_υ and integration domain Ω_Q for node i; interpolation domain Ωi for Gauss integration point x_Q.

3.3. Boundary conditions

Variety of boundary conditions may be considered by the combination of simply-supported (S), clamped (C) and free (F) edges. For instance, the following boundary conditions are taken

Simply supported -Simply supported (SS)

$$v = w = \psi_\theta = M_x = N_x = 0, \qquad \text{at edges } x = 0, x = L \tag{30}$$

Clamped-Clamped (CC)

$$u = v = w = \psi_x = \psi_\theta = 0, \qquad \text{at edges } x = 0, x = L \tag{31}$$

Clamped-Free (CF)

$$\begin{aligned} &u = v = w = \psi_x = \psi_\theta = 0, && \text{at edge } x = 0 \\ &N_x = N_{x\theta} = M_x = M_{x\theta} = Q_x = 0, && \text{at edge } x = L \end{aligned} \tag{32}$$

4. Results and discussion

The comparison of results from the present numerical method and exact solution for the isotropic cylindrical shell with simply supported ends is shown in Figure 4. ($\frac{R}{h} = 100, E = 7.2e10\frac{N}{m^2}, \rho = 2700\frac{kg}{m^3}, \nu = 0.27$) . Good agreement is achieved that shows the ability and accuracy of present method. Figure 5 is presented to study the convergence of the critical axial buckling load of an isotropic shell with simply supported ends over a wide range of aspect ratio (the ratio of length to radius) for different number of nodes in the problem domain. The effects of geometrical parameters are graphed in Figure 6. As the ratio of radius to thickness is increased, the critical buckling loads tend to decrease. In Figure 7, the influence of boundary conditions on the critical buckling load is clearly demonstrated. According to this figure, in the limited area of length-to-radius ratio, for example between 0.1 to 90 for a simply supported shell, the buckling load is almost independent of this ratio but in greater ratios the load is strongly sensitive. Figure 8 is presented to show the influence of different weight functions for instance the cubic and quartic spline functions and exponential weight function which are used in present meshless method. Obviously, by applying the quartic spline weight function in the MLPG formulation, the axial buckling load is decreased and there is less agreement between the exact solution and the numerical solution by using other weight functions.

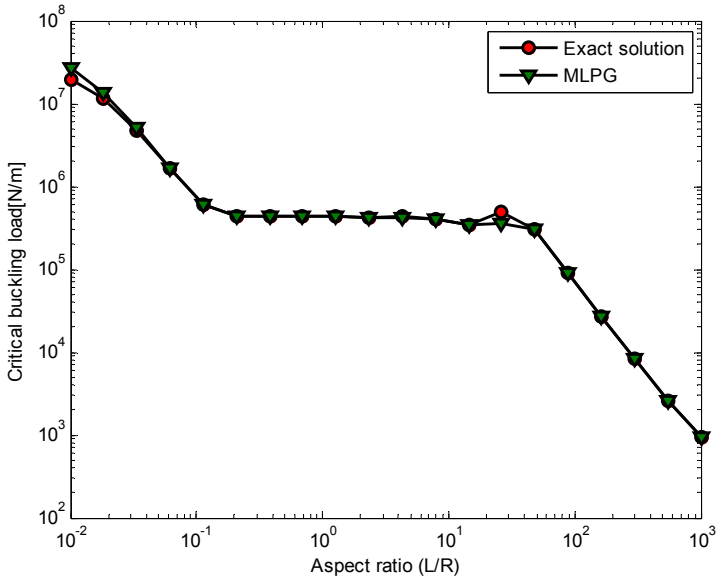

Figure 4. Comparison of MLPG method with exact solution.

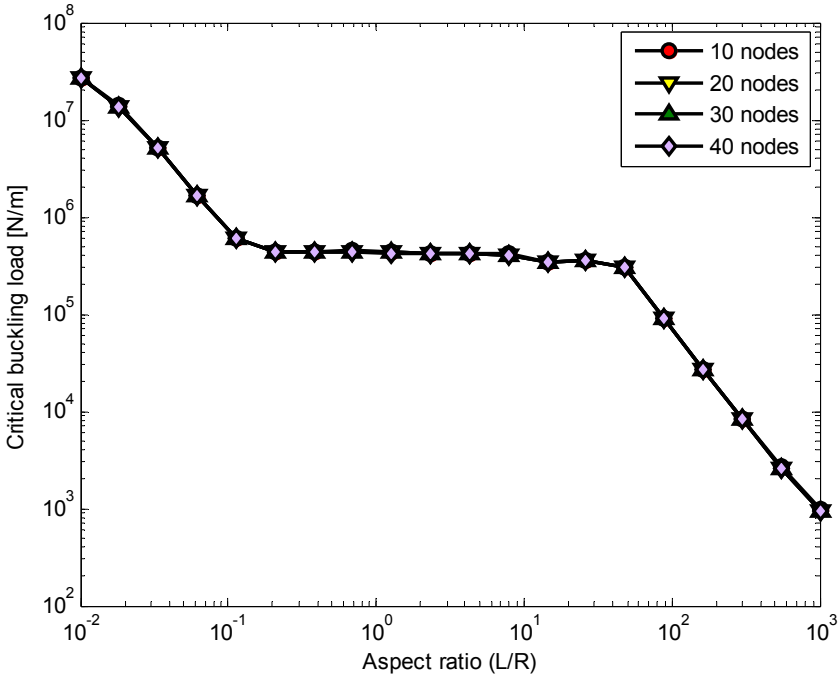

Figure 5. Convergence of the critical buckling load for simply supported shell.

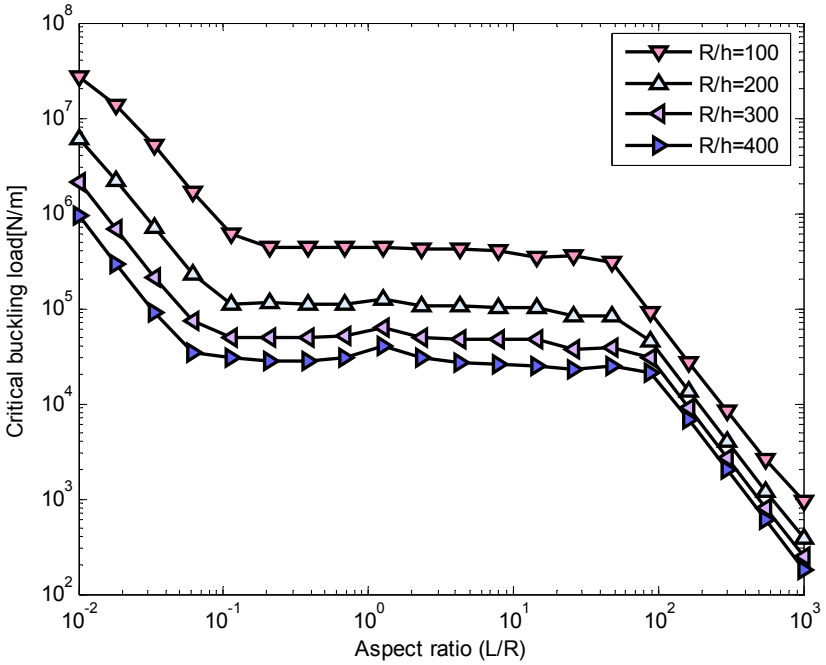

Figure 6. Influence of geometrical parameters on critical buckling load.

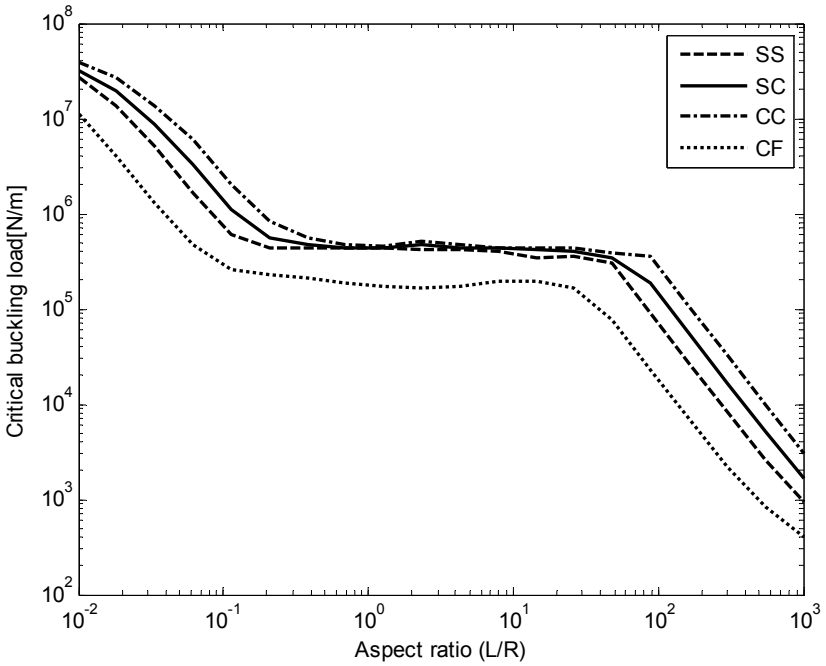

Figure 7. Influence of boundary conditions on critical buckling load.

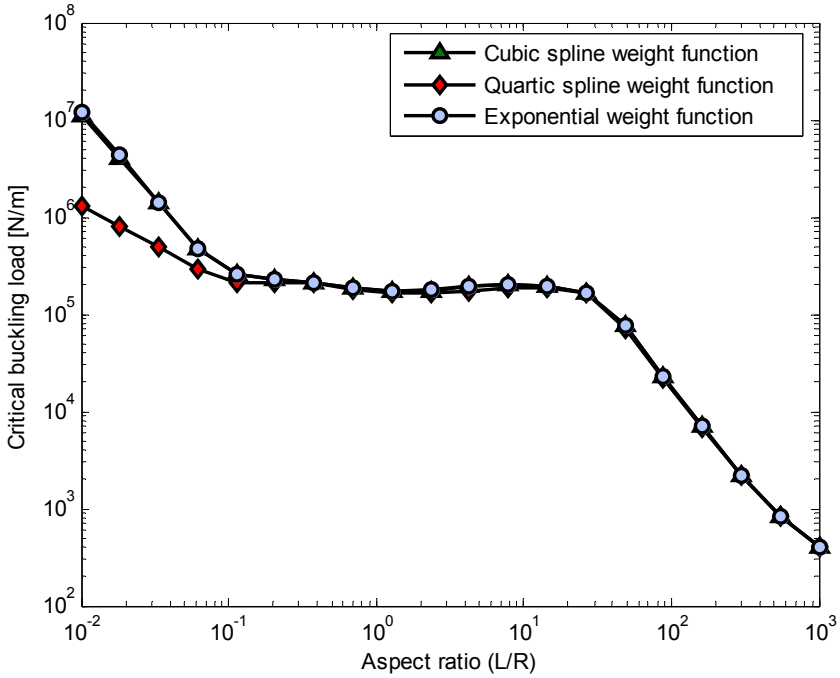

Figure 8. Influence of various weight functions on critical buckling load.

5. Conclusion

The axial buckling of isotropic cylindrical shell with different boundary conditions was studied in this article. The governing equations were developed based on the Donnell theory and then the variational form of the field equations was constructed by applying semi-inverse methods. The meshless local Petrov-Galerkin method was used to solve them numerically. The present method was successfully adopted to study the axial buckling of shell .The influences of different boundary conditions, geometrical parameters and the effects of using various weight functions were fully investigated which clearly show the accuracy of the present method.

References

[1] R.A. Gingold, J.J. Monaghan, Smoothed particle hydrodynamics: theory and application to non-spherical stars, *Mon. Not. Roy. Astron. Soc.,* 181 (1977) 375-389.

[2] B. Nayroles, G. Touzot, P. Villon, Generalizing the finite element method: diffuse approximation and diffuse elements, *Computational Mechanics*, Vol. 10, 5 (1992) 307–318.

[3] T. Belytschko, Y.Y. Lu, L. Gu, Element-free Galerkin methods, *International Journal for Numerical Methods in Engineering*, Vol. 37, 2 (2005) 229–256.

[4] W.K. Liu, S. Jun, Y. Zhang, Reproducing kernel particle methods, *International Journal for Numerical Methods in Fluids*, Vol. 20, 8-9 (2005) 1081–1106.

[5] C.A. Duarte, J.T. Oden, An h-p adaptive method using clouds, *Computer Methods in Applied Mechanics and Engineering*, Vol. 139, 1-4 (1996) 237–262.

[6] I. Babuska, J. Melenk, The partition of unity method, *International Journal for Numerical Methods in Engineering*, Vol. 40, 4 (1998) 727–758.

[7] N. Sukumar, B. Moran, T. Belytschko, The natural element method in solid mechanics, *International Journal for Numerical Methods in Engineering*, Vo. 43, 5 (1998) 839–887.

[8] S.N. Atluri, T. Zhu, A new meshless local Petrov–Galerkin (MLPG) approach in computational mechanics, *Computational Mechanics*, Vol. 22, 2 (1998) 11–27.

[9] S.N. Atluri, *The Meshless Local Petrov-Galerkin (MLPG) Method for Domain & Boundary Discretizations*, Tech Science Press, 2004.

[10] S.N. Atluri, S. Shen, The meshless local Petrov-Galerkin (MLPG) method: a simple & less-costly alternative to the finite element and boundary element methods, *Tech Science Press*, Vol.3, 1 (2002) 11-51.

[11] S.N. Atluri, S. Shen, The basis of meshless domain discretization: the meshless local Petrov–Galerkin (MLPG) method, *Advances in Computational Mathematics*, Vol. 23, 1-2 (2005) 73–93.

[12] M.N. Naeem, Prediction of natural frequencies for functionally graded cylindrical shells, *Ph.D. Dissertation*, UMIST, UK, 2004.

[13] S. Adali, Variational principles for multi-walled carbon nanotubes undergoing buckling based on nonlocal elasticity theory, *Physics Letter A*, Vol. 372, 35 (2008) 5701–5705.

[14] J.H. He, Variational principles for some nonlinear partial differential equations with variable coefficients, *Chaos, Solitons& Fractals*, Vol. 19, 4 (2004) 847-851.

[15] J.H. He, Variational approach to (2+1)-dimensional dispersive long water equations, *Physics Letters A*, Vol. 355, 2-3 (2005) 182-184.